Int. J. Electrochem. Sci., 16 **(2021)** Article ID: 21046, doi: 10.20964/2021.04.24

International Journal of
ELECTROCHEMICAL
SCIENCE
www.electrochemsci.org

NSGA-II Optimized Multiobjective Predictive Energy Management for Fuel Cell/Battery/Supercapacitor Hybrid Construction Vehicles

Huiying Liu[1], *Xiaoxue Xing*[1], *Weiwei Shang*[1], *Tianyu Li*[2,*]

[1] College of Electronic Information Engineering, Changchun University, 130022 Changchun, China
[2] School of Mechanical and Aerospace Engineering, Jilin University, 130025 Changchun, China
[*]E-mail: litianyu@jlu.edu.cn

Received: 2 December 2020 / *Accepted:* 20 January 2021 / *Published:* 28 February 2021

Fuel cell/battery/supercapacitor hybrid vehicles have shown good prospects. Energy management strategies (EMSs) are proposed to solve the complex energy management issues associated with the fuel cells/batteries/supercapacitors of construction vehicles, and to optimised economy and performance. Here, we develop a multiobjective predictive EMS. In the predictive control framework, a non-dominated sorting genetic algorithm (NSGA-II) enhances fuel cell and battery durability while minimising economic cost. NSGA-II optimises cost functions in real-time and generates a Pareto front, the data of which are screened by fuzzy logic algorithm to obtain optimal control solutions. Simulations indicated the superior feasibility and effectiveness of our proposed EMS compared to conventional benchmarks. The EMS ensures that fuel cell/battery/supercapacitor hybrid construction vehicles not only receive adequate power under complex working conditions, but also reasonably distribute the power demand among fuel cells/batteries/supercapacitors; this extends the lifespan of these devices and ensures high efficiency.

Keywords: fuel cell; hybrid system; energy management; model predictive control; multiobjective optimization.

1. INTRODUCTION

The extensive emissions of construction vehicles, including loaders, bulldozers, forklifts, scrapers, and excavators, are of concern. Given the global energy crisis and global warming, fuel cell vehicles (FCVs) are increasing in popularity because they exhibit efficient energy conversion and are environmentally friendly [1]. Fuel cell hybrid construction vehicles (FCHCVs) benefit from compact size, high energy conversion efficiency, zero pollution, and quiet operation [2]. Commercial fuel cells have many applications [3,4]. The global FCVs market is expected to reach US$24.81 billion by 2025 [5]. FCHCVs exhibit remarkable potential.

The dynamic performance and lifetime of a fuel cell depend on the peak power demands and frequency of power variations. Fuel cells alone cannot recover energy. Thus, hybrid powertrains have been developed for vehicular applications. Fuel cells are linked to auxiliary energy storage systems (AESSs), which can be in the form of a battery pack, supercapacitor, or combination thereof [6]. Generally, batteries exhibit higher specific energy but lower specific power compared to supercapacitors [7,8]. A combination battery/supercapacitor, such as an AESS, is recommended for vehicular applications; such combination devices exploit the high energy density of batteries and supercapacitors [9]. If a supercapacitor is employed, battery power can be reduced, thus prolonging battery lifetime. Here, we discuss FCHCVs with AESSs equipped with batteries/supercapacitors. Given the different dynamics of the three power sources, an energy management strategy (EMS) is essential to coordinate the energy distribution, thus improving system performance and economy [10]. EMS development has become an important research topic. The working environment of a construction vehicle is complex; the loads change frequently and significantly, severely testing the EMS of the three energy sources.

An FCHCV EMS operates under complex conditions. Research has turned from rule-based to optimisation-based EMSs [11]. Rule-based EMSs relying on design experience are often easy to implement [12]; optimisation theory-based strategies tend to be more complex but also more effective. Rule-based EMSs feature state machine [13], operation mode [14], sliding mode variable structure control [15], state machine strategy [16], and fuzzy logic control strategies [17,18]. Fuzzy control tolerates mathematical and data imprecision, and robust performance in terms of real-time FCHEV control [19]. The advantages of rule-based EMSs include the classification of operating models, the use of real-world engineering knowledge, and high static energy efficiency. Rule-based EMSs do not require precise performance data and are both robust and deductive, effectively and simply allocating power. However, rule-based EMSs rely heavily on operator experience, and do not necessarily optimise the global strategy. Thus, optimisation-based approaches have emerged including global and local algorithms. The former method involves convex optimisation [20], dynamic programming [21], heuristic dynamic programming [22], and genetic or other optimisation algorithms [23]. These EMSs aim to obtain optimal global strategies but impose a heavy computational burden and require a thorough knowledge of drive cycle features. However, real-time (local) EMSs including Pontryagin's minimum principle (PMP) [24], the equivalent consumption minimisation strategy (ECMS) [25,26], or model predictive control (MPC) [27,28] do not require specific drive cycle data or impose a heavy calculation burden, but yield only local optimal real-time energy distributions. Many scholars used the PMP to develop near-optimal strategies for hybrid FCVs. However, the models do not work well in the real world. MPC-based EMSs have thus received a great deal of attention [29,30]. MPC based EMS has become research hotspot in vehicle energy management. We have explored MPC-based EMSs for FCHCVs, and achieved some significant results [31,32]. However, the EMSs of fuel cell/battery/supercapacitor hybrid system needs further study.

The EMSs of FCVs must solve multiobjective optimisation problems (MOPs), minimise energy use and emissions, optimise power use, and maximise fuel cell and battery lifetimes. Genetic[33], particle swarm [34], and other optimisation algorithms have been used to derive multiple solutions to large MOPs simultaneously. An multiobjective optimization system delivers Pareto solutions or non-dominated solutions [35]. Many authors have focused on multiobjective optimization controllers, using

multimodal strategies to develop multiobjective optimization, multi-population genetic and artificial fish swarm algorithms [36–38]. The non-dominated sorting genetic algorithm (NSGA) is an multiobjective optimization, and NSGA-II improves on the original it [39]. It is essential to minimise overshoot and the settling times of all MOP solutions. Conventional MPCs are improved by NSGA-II [40].

The main contribution of this study is the energy management development for FCHCVs powered by fuel cells/batteries/supercapacitors hybrid system. According to the characteristics of the three power sources, appropriate energy management strategies are studied based on system mathematical model. EMSs can dynamically adjust the output of fuel cell/battery/supercapacitor, to reduce the hydrogen consumption of fuel cell, improve the system energy utilization and system efficiency, and improve the fuel cell and battery durability. The complex working conditions is one of the basic problems to be solved in the FCVs. It is important to study the influence of complex working conditions on the performance fuel cell and battery. The research has significance for various fuel cell hybrid system. To solve the complex power distribution of the three nonlinear power sources, a new predictive control framework-based energy management is proposed. The energy management is a complex multiobjective optimisation problem considering vehicle economy and performance at the same time. NSGA-II is used for optimisation of the multiobjective energy management problem, and generates a Pareto front to obtain optimal control solutions. Finally, this paper is as follows: the FCHCV model is established in Section 2. The predictive EMS is proposed in Section 3. Simulations are discussed in Section 4. Conclusions are Summarized in Section 5.

2. PROBLEM STATEMENT

2.1 The FCHCV

We studied an FCHCV with a powertrain featuring a fuel cell/battery/supercapacitor (Figure. 1). FCHCV is powered by a fuel cell stack (FCS), a battery pack, and a supercapacitor module. The FCS is connected to the DC bus via a boost direct current (DC)/DC converter. The battery pack and supercapacitor module are connected via bidirectional DC/DC converters. One motor is used to drive the vehicle; The other motor drives the hydraulics used for bucket operation and steering.

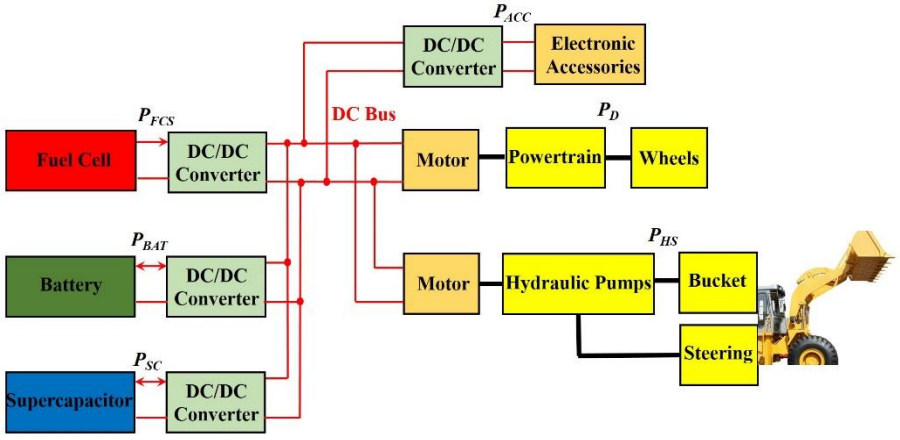

Figure 1. Topology of the FCHCV.

In Figure. 1, P_D and P_{HS} is the power of the traction and hydraulic system, respectively. P_{FCS}, P_{BAT}, and P_{SC} denote the power of the FCS, the battery pack, and the supercapacitor module, respectively.

2.2 Powertrain and hydraulic system models

Below, we develop the FCHCV model. The principal FCHCV loads are the powertrain, hydraulic system, and vehicle electronic load P_{ACC} (which is random and treated as a constant 5 kW). In the real world, road conditions and bucket operation vary. The powertrain load calculation is based on dynamics, and the hydraulic load is derived using hydraulic principles. The model is simple:

$$P_D = \left(G \cdot \left(\sin\theta + f \cdot \cos\theta \right) + K_A \cdot S \cdot \left(v - v_w \right)^2 + \delta \cdot m \cdot \frac{dv}{dt} \right) \cdot v \qquad (1)$$

$$P_{HS} = \sum_{i=1}^{i=k} \frac{p_i \cdot q_i \cdot n_i}{60 \cdot \eta_i} \qquad (2)$$

where G is the overall quality, f and K_A are coefficients, θ is the road grade, S is the front area, v is the speed, v_w is the wind speed, and δ is a conversion factor for the rotating mass. p_i, q_i, η_i, and n_i refer to the pressure, flow rate, efficiency, and rotational speed of a hydraulic pump; there are k hydraulic pumps.

2.3 Fuel cell model

The FCS used proton exchange membrane fuel cell (PEMFC) [41]. The dynamics of a single fuel cell are calculated as follows:

$$V_{cell} = E_{cell} - V_{act} - V_{ohm} \qquad (3)$$

$$\begin{cases} E_{cell} = E_0 - k_c \cdot e^{-3} \cdot \left(T - T_C \right) + \dfrac{R_C \cdot T}{2F} \cdot \ln\left(\sqrt{P_{O2}} \cdot P_{H2} \right) \\ V_{act} = \dfrac{R \cdot T}{2\alpha \cdot F} \cdot \ln \dfrac{I_{FC}}{I_0 \cdot S_{cata}} \\ V_{ohmic} = I_{FC} \cdot R_{\text{int}} \end{cases} \qquad (4)$$

where E_{cell} denotes the electromotive potential, I_{FC} is the FCS current, V_{act} are the losses caused by cell activation, and V_{ohm} are the losses caused by cell internal resistance. T is the temperature, T_C is the temperature offset. R_C and F are gas constant and Faraday constant. P_{O2} and P_{H2} are the pressures at the interfaces of the cathodic and anodic catalytic layers respectively. E_0 and k_c are constants. α is the charge transfer coefficient, I_{FC} is the fuel cell current in amperes, S_{cata} is the catalyst layer section area, and I_0 is the exchange current density.

Finally, the electrical output power can be obtained as:

$$P_{FCS} = N_{cell} \cdot V_{cell} \cdot I_{FC} \qquad (5)$$

$$\dot{m}_{H2FC} = N_{cell} \cdot \frac{M_{H2}}{ne \cdot F} \cdot I_{FC} \qquad (6)$$

where N_{cell} denotes the number of cells in the stack. m_{H2FC}, M_{H2}, and *ne* denote the hydrogen consumption, molar mass of hydrogen, and number of electrons, respectively.

2.4 Battery model

Batteries are widely used to store energy in electric vehicles [42]. In an EMS, the battery parameters must reflect the working status. Li-ion batteries are often used in high-performance vehicles. The cost of these batteries is falling and performance is improving; literature models are available [43]. We used a simple PNGV model [44,45]:

$$U_{BAT} = U_{OCV} - I_{BAT} \cdot R_{BAT} - U_{PBAT} \quad (7)$$

$$P_{BAT} = U_{BAT} \cdot I_{BAT} \quad (8)$$

$$SoC_{BAT} = SoC_{BATInit} - \int \frac{I_{BAT}}{Q_{BAT}} dt \quad (9)$$

where SoC_{BAT} denotes the battery state of charge (SoC). U_{OCV} and U_{PBAT} denote the ideal open-circuit and polarisation voltages, respectively. I_{BAT} and R_{BAT} denote the load current and internal resistance, respectively.

2.5 Supercapacitor model

We used a supercapacitor to manage the power produced by, and demanded from, the FCS and battery; a supercapacitor provides high power density, fast charging, rapid power release, and a very long life cycle. In the absence of a supercapacitor, the FCS and battery would be required to manage the entire workload even at high peak power, thus degrading their lifespan or increasing their size and cost [46,47]. A supercapacitor delivers energy very rapidly, which is important if the power demand varies frequently. Many different models employing the RC circuit are available; we used the following equivalent supercapacitor model [48]:

$$P_{SC} = U_{SC} \cdot I_{SC} \quad (10)$$

$$I_{SC} = \frac{U_{SC} - \sqrt{U_{SC}^2 - 4R_{SC} \cdot P_{SC}}}{2R_{SC}} \quad (11)$$

$$SoC_{SC} = \frac{U_{SC}}{U_{SC\max}} \quad (12)$$

where SoC_{SC} denotes the supercapacitor SoC, and I_{BAT}, U_{SC}, and R_{SC} is the operating current, ideal open-circuit voltage, and internal resistance, respectively. U_{SCmax} denotes the maximum open-circuit voltage.

2.6 DC/DC convertor model

Converters are important for energy management, regulating the output voltage and current. It is assumed that the time constants of the inductors within the DC/DC converters are much larger than the

switching period. Therefore, it is reasonable to use an equivalent static model of a DC/DC converter [49]:

$$V_{OUT}=\frac{1}{\kappa_{DC}}\left(V_{IN}-L\frac{dI_L}{dt}-I_L\cdot R_L\right) \quad (13)$$

$$I_{OUT}=\begin{cases}\kappa_{DC}\cdot I_L\cdot\eta_{DC}, \text{boost mode}\\ \dfrac{\kappa_{DC}\cdot I_L}{\eta_{DC}}, \text{bidirectional mode}\end{cases} \quad (14)$$

where V_{IN} and V_{OUT} denote the input and output voltage, respectively. R_L denotes the resistor of the inductor; L is the inductance and κ_{DC} is the output to input voltage ratio. I_L and I_{OUT} are the current through the inductor and output current of the converter, respectively. η_{DC} is the converter efficiency.

3. DEVELOPMENT OF THE NSGA-II OPTIMISED MO-PREDICTIVE EMS

3.1 EMS development

An MPC has the advantages of rolling optimisation and feedback correction, and exhibits good dynamic control; an MPC is ideal for vehicle energy management[50–52]. On this basis, energy management is optimised in terms of low fuel consumption and emission levels. In this section, we develop a classical predictive EMS for an FCHCV based on MPC theory. The control framework is illustrated in Figure. 2.

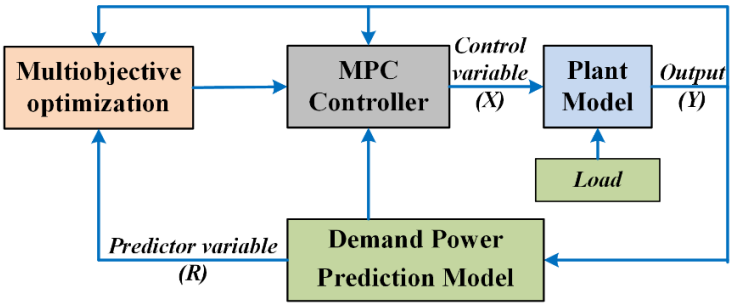

Figure 2. Control framework of the EMS.

In the control framework as shown in Figure. 2, $X=[\{P_{BAT}^*\}_{CL}, \{P_{SC}^*\}_{CL}]$, $R=\{P_{Load}^*\}_{PL}$. X is the system control variable, that is, the predictive controller gives the control variable sequences of battery power P_{BAT}^* and supercapacitor power P_{SC}^* in the control domain length CL. Y is the output of the system model, which contains many vehicle state parameters.

The predicted parameter is the vehicle future power demand, which is the sum of vehicle electronic load, powertrain load, and hydraulic load. P_{Load}^* is the predicted power sequences in the prediction domain length PL, which is predicted using a neural network model on the basis of historical information as proposed in literature [2]. The input of the prediction model is the historical demand

power, and the output is the future power demand. The model predicts future power demand in real-time.

The proposed EMS aims to comprehensively improve FCHCV performance. Given the multiple optimisation objectives, the optimal control variables of the supercapacitor power and battery power are calculated using an multiobjective optimization algorithm. The control framework is essentially a rolling optimisation process based on MPC theory. The multiobjective optimization objectives of the EMS include minimisation of hydrogen consumption; establishment of reasonable SoC ranges for the battery and supercapacitor; avoidance of large currents and frequent current variations (to improve FCS durability); avoidance of deep SoC discharge and large currents (to prolong battery durability); and minimisation of real-time costs, as expressed mathematically below:

$$\min J = \left[J_1, J_2 \right] \tag{15}$$

$$\begin{cases} J_1 = P_{ric} \cdot \left(m_{H2FC} + em_{H2} \right) + C_{OSTOP} \\ J_2 = w_1 \cdot \left(SoC_{BAT} - SoC_{BATmid} \right)^2 + w_2 \cdot \left(SoC_{SC} - SoC_{SCmid} \right)^2 + w_3 \cdot I_{FC} + w_4 \cdot \left| I_B \right| \end{cases} \tag{16}$$

$$em_{H2} = \frac{P_{SC} \cdot \lambda_{SC} + P_{BAT} \cdot \lambda_{BAT}}{\overline{\eta_{FC}} \cdot \overline{\eta_{DC}} \cdot q_{H2}}$$

$$\begin{cases} \lambda_{SC} = \overline{\eta_{DC}}, \text{boost mode} \\ \lambda_{SC} = \dfrac{1}{\eta_{DC}}, bidirectional \text{ mode} \end{cases} \tag{17}$$

$$\begin{cases} \lambda_{BAT} = \overline{\eta_{DC}}, \text{boost mode} \\ \lambda_{BAT} = \dfrac{1}{\eta_{DC}}, bidirectional \text{ mode} \end{cases}$$

$$C_{OSTOP} = P_{ric} \cdot k_{H2FC} \cdot m_{H2FC} \tag{18}$$

where J_1 and J_2 are the optimisation objectives. em_{H2} denotes the equivalent hydrogen consumption, P_{ric} denotes the price of hydrogen, and k_{H2FC}, w_1, w_2, w_3, and w_4 are coefficients. SoC_{BATmid} and SoC_{SCmid} represent the median SoCs of the battery and supercapacitor, respectively. $\overline{\eta_{FC}}$ and $\overline{\eta_{DC}}$ is the average efficiency of the FCS and DC/DC converter, respectively. q_{H2} denotes the calorific value of hydrogen. In this study, the w_1, w_2, w_3, and w_4 are set as 1, 1, 0.00001, and 0.00001. These coefficients have a certain influence on the optimization results. However, they have little influence on the superiority and effectiveness of EMS evaluation. The coefficients can be adjusted according to the actual model parameters for different vehicles.

When solving the EMS problem, several constraints must be observed:

$$\begin{cases} SoC_{SC} \in \left[SoC_{SC\min}, SoC_{SC\max} \right] \\ SoC_{BAT} \in \left[SoC_{BAT\min}, SoC_{BAT\max} \right] \\ I_{SC} \in \left[I_{SC\min}, I_{SC\max} \right] \\ I_{BAT} \in \left[I_{BAT\min}, I_{BAT\max} \right] \\ P_{FC} \in \left[P_{FC\min}, P_{FC\max} \right] \\ \left| P_{FC} - P_{FClast} \right| \le P_{FCS\,Rate} \end{cases} \tag{19}$$

where SoC_{BATmax}, SoC_{BATmin}, SoC_{SCmax}, and SoC_{SCmin} are the SoC constrains. I_{BATmax}, I_{BATmin}, I_{SCmax}, and I_{SCmin} are the currents constrains. P_{FCmax} and P_{FCmin} denote the limits of FCS power. P_{FClast} denotes the FCS power at the last moment in time.

Our predictive EMS is used to achieve two independent objectives. The first objective is real-time cost reduction; this considers the costs of FCS hydrogen consumption, battery and supercapacitor (equivalent) hydrogen consumption, and FCS operation. This function reflects the real-time hydrogen consumption and operation costs of the FCHCV. The second objective function includes the SoC operating range, battery current, and FCS current constraints. By limiting the FCS power and power change rate, FCS durability is enhanced. By limiting the battery SoC (thus avoiding overcharging or undercharging), the operating range, and the working current, battery durability is improved.

3.2 NSGA optimization algorithm

As mentioned above, our EMS needs to solve an multiobjective optimization problem. It is nearly impossible to find a solution that optimises all objectives. Often, several conflicting objectives should be optimised; a multiobjective optimization yields a set of best solutions rather than the single solutions of traditional multiobjective optimization weighting and ε-constraint methods; these provide non-dominated solutions or Pareto fronts [53]. Multiobjective global optimisation aims to obtain the Pareto front and then chooses a variety of solutions. A genetic algorithm can be adopted to this end. Many such algorithms can be used to solve multiobjective optimization problems in engineering [54,55]. Among the most popular of these algorithms is the global multiobjective optimization optimisation algorithm NSGA-II, which handles convergence and diversity metrics better than other topologies [56]. Unlike the traditional multiobjective optimization weighting and ε-constraint methods, NSGA-II cannot be affected by constraints or weights [57]. Therefore, we used NSGA-II to optimise our MPC-based EMS. Formula (15) presented the objective, and the control parameters were the optimisation (decision) variables. The optimisation problem was constrained by formula (19). The NSGA-II algorithm is elitist; the sharing function is replaced by the crowding distance and there is no need to specify a sharing parameter [36]. The pseudo-code of the optimization algorithm is shown in Algorithm 1.

Algorithm 1. Pseudo-code for the optimization algorithm.

Input: Population size *N*, probability of crossover and mutation, mutation strength
Output: All the optimal solutions (Pareto front of solutions)

```
Initialize population and iteration number
while Termination criteria are not achieved
   repeat for each solution
   Perform genetic operations
   Evaluate fitneess
   Rank all solutions based on dominance
   Calculate crowding distance
   while Population size<N
     Select solutions based on crowding distance
   end
end
return
```

After obtaining Pareto front, the optimal solution needs to be selected from the solution set. How to choose the optimal solution needs to be combined with the vehicle state. Different load and SoC condition require different tendentiousness between J_1 and J_2. Formula (20) is the selection principle used in this paper. It is important to set an appropriate weight to reflect the priority of the objectives properly. An optimal solution selection method based on fuzzy logic model is adopted to adjust the weight dynamically. The fuzzy logic model is shown in Figure.3. The inputs are the normalized load, battery SoC, and supercapacitor SoC; the output is the weight.

$$\left\{P_{BATopt}, P_{SCopt}\right\} = \min\left\{\varphi \cdot J_{1Pa}\left(P_{BAT}, P_{SC}\right) + \left(1-\varphi\right) J_{2Pa}\left(P_{BAT}, P_{SC}\right)\right\}_{num} \quad (20)$$

where P_{BATopt} and P_{SCopt} denote the optimal battery and supercapacitor control power, respectively. J_{1Pa} and J_{2Pa} are the cost function values of the Pareto front solution set. *num* is the number of solution set.

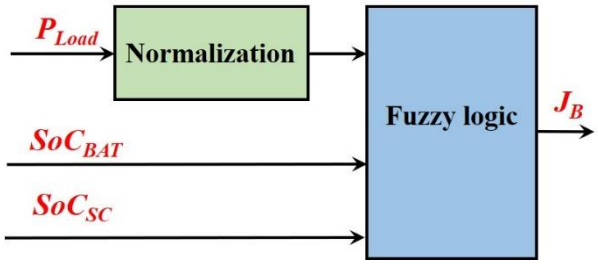

Figure 3. Structure of the fuzzy logic model for weight φ.

3. RESULTS AND DISCUSSION

Here, we describe EMS optimisation and simulation. We compared our EMS to other representative EMSs via simulation of a driving cycle of a ZL50 wheel loader (Figure. 4) [58]. Figure. 4 describes the vehicle speed and hydraulic system pressures in the process of a V-shaped operation. The total operation time is about 90s, which includes five stages: approach the material; shovel; reverse; unload; reverse and return to the starting point. The FCHCV specifications are listed in Table 1. The predictive horizon length of the EMS is five steps, and the control horizon length is three steps (0.1 s/step). Simulations were performed using MATLAB (MathWorks, Inc., Natick, MA, USA).

Table 1. FCHCV specifications

Specifications	Value
Vehicle mass	16800 kg
Maximum speed	37 km/h
FCS	100 kW
Battery pack	400 V / 5.28 kWh
Li-ion battery cell	2.2 Ah/ 3.2 V
Supercapacitor pack	500V / 15.75F
Supercapacitor cell	3000 F / 2.7 V

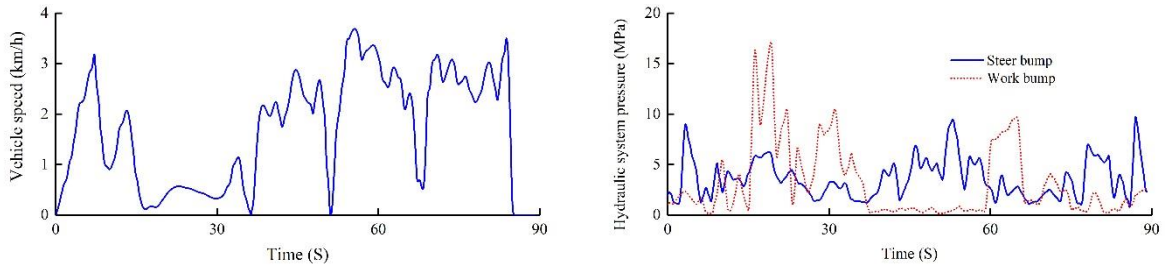

Figure 4. Representative driving cycle of FCHCV. (a) Vehicle speed; (b) Hydraulic system pressures.

4.1 Optimization algorithm performance

In this section, we discuss the optimisation achieved by NSGA-II, especially the speed of attainment of the Pareto front. NSGA-II parameters used in optimization are presented in Table 2 [59]. We explored whether the NSGA-II-derived Pareto front was optimal by evaluating the objective functions J_1 and J_2 in terms of the control parameters P_{BAT} and P_{SC}; the results of once calculation are shown in Figure. 5 (together with the Pareto front). It is evident that NSGA-II provided the optimal trade-off between the objectives. We prioritised J_1, i.e. the cost of operation. We used the Pareto solution that achieved the priority cost and certain performance by weighting method [32].

Table 2. NSGA-II parameters used in optimization

Parameters	Value
Population size	50
Selection	2
Crossover	0.9
Mutation	Adaptive
Pareto fraction	0.35
Stop criteria	100 generations

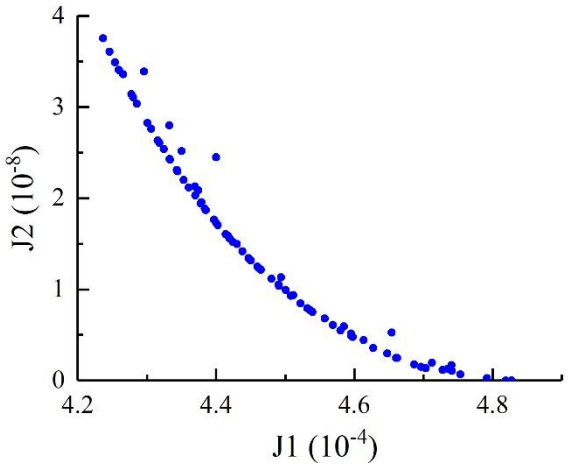

Figure 5. Optimization results of NSGA-II.

To evaluate the NSGA-II more deeply, the Pareto solutions of the proposed NSGA-II-optimized EMS are tested on a representative load fluctuation condition as shown in Figure.4 (10-20 s), where the load fluctuates between about 55-80 kW and takes about 10 s. The weighing between J_1 and J_2 needs testing. The Pareto solutions are tested in different emphasis on J_1 and J_2. Figure. 6 is informative to this end. For cost priority (J_1 priority), the optimal solutions implement good J_1 and J_2 together. The battery contribution is strongly loaded at the initial stage and battery SoC fall quickly, whereas the supercapacitor charges so that the supercapacitor SoC reaches upper. After about 3 s, the supercapacitor provide the required power alone, and battery charges slowly to restore SoC balance. On the contrary, for SoC balance priority (J_2 priority), the optimal solutions implement no better than the other two types. The battery charges quickly so that battery SoC can be balanced as soon as possible. For the balanced weight, it gives good performances between cost priority and SoC balance priority methods. Therefore, weight selection plays an important role in tuning parameter for the EMS.

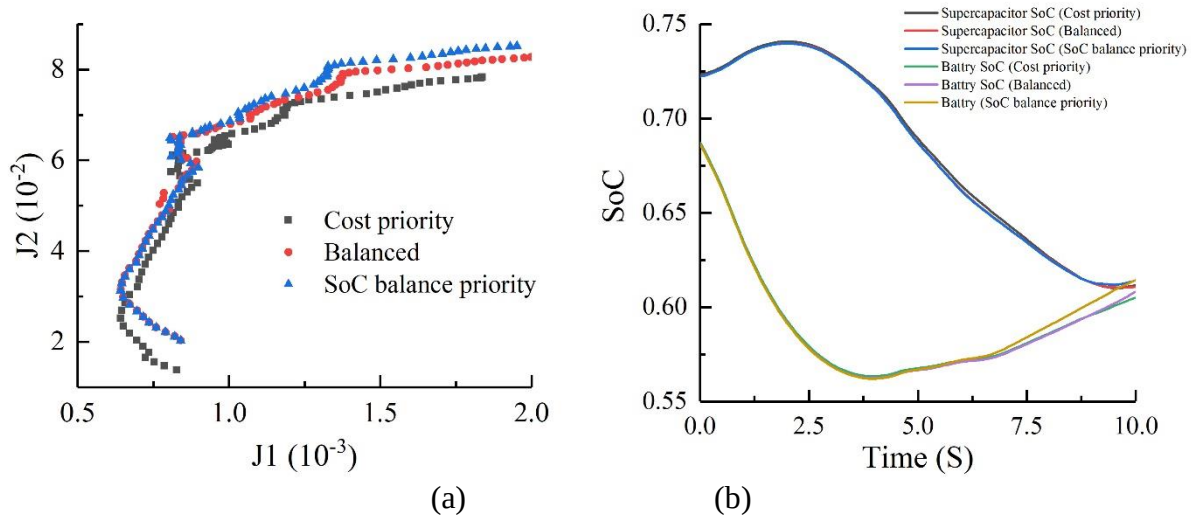

Figure 6. Optimization results of the EMS over load fluctuation condition. (a) Distribution of cost function corresponding to optimal solution; (b) Supercapacitor SoC and battery SoC.

4.2 The EMS

We compared our predictive EMS to frozen-time MPC (FMPC) and prescient MPC (PMPC) based EMSs as described in the literature [29] in the simulation. The former adopts the constant prediction. The latter is a typical benchmark algorithm that exploits a priori knowledge of future loads to optimally deal with the control problem. Simulations are performed using three representative driving cycles as shown in Figure. 4, and simulation results are shown in Figures. 7–11.

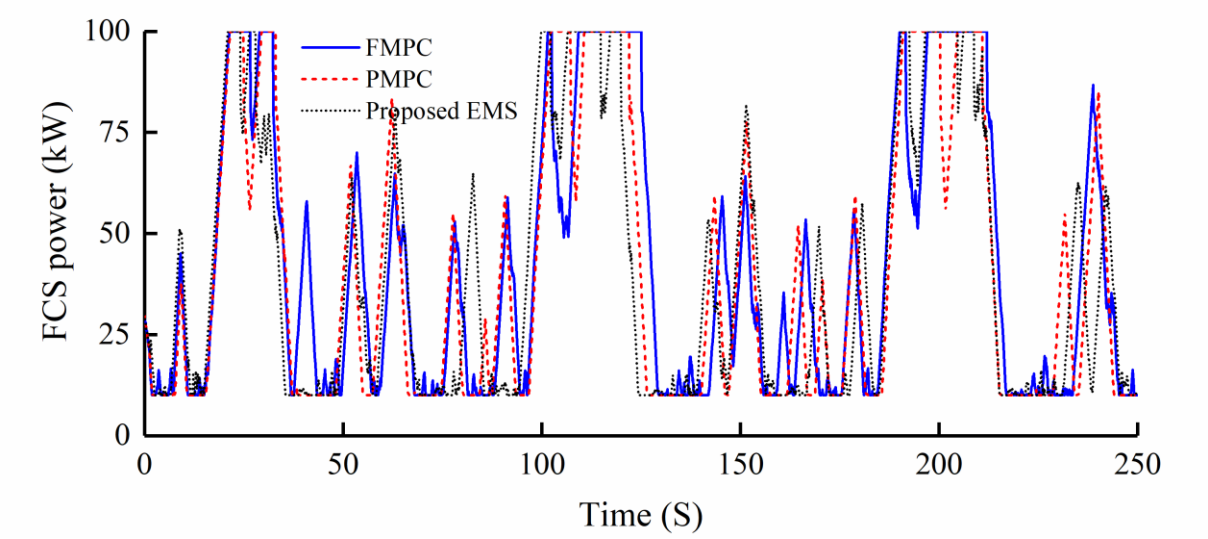

Figure 7. FCS power

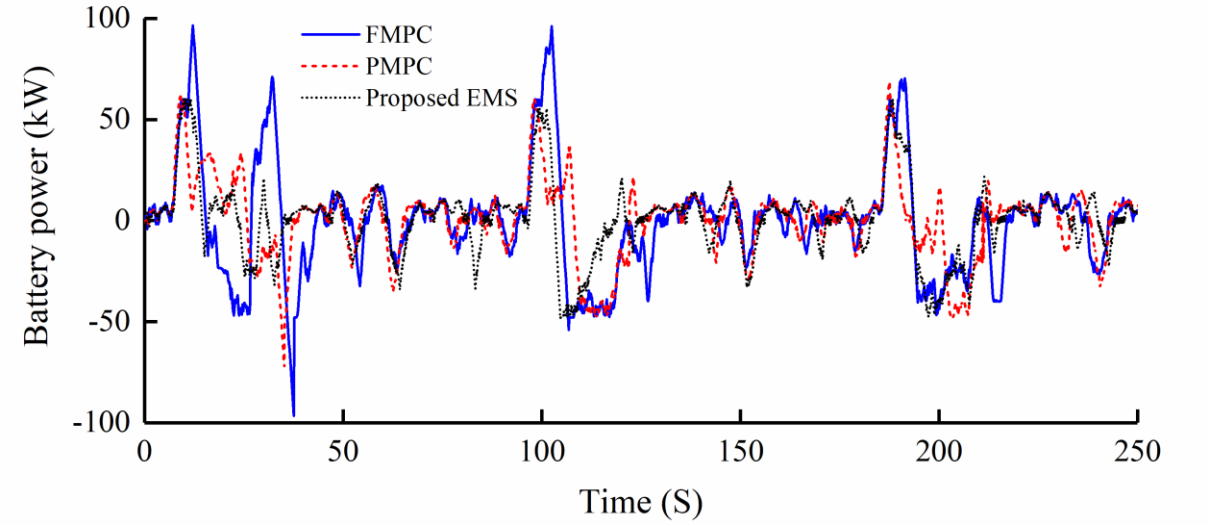

Figure 8. Battery power

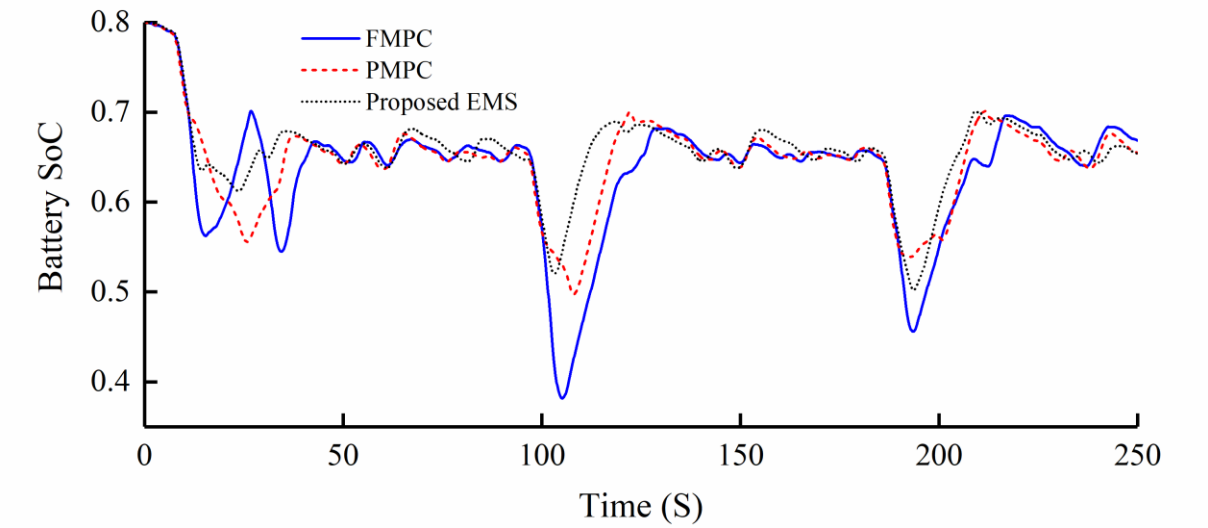

Figure 9. Battery SoC

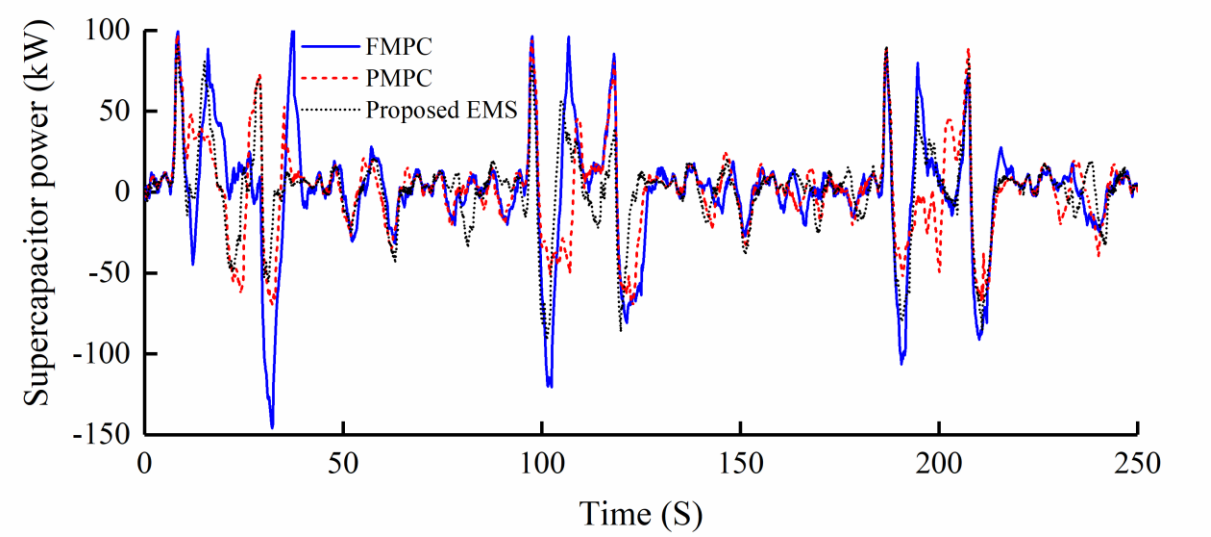

Figure 10. Supercapacitor power

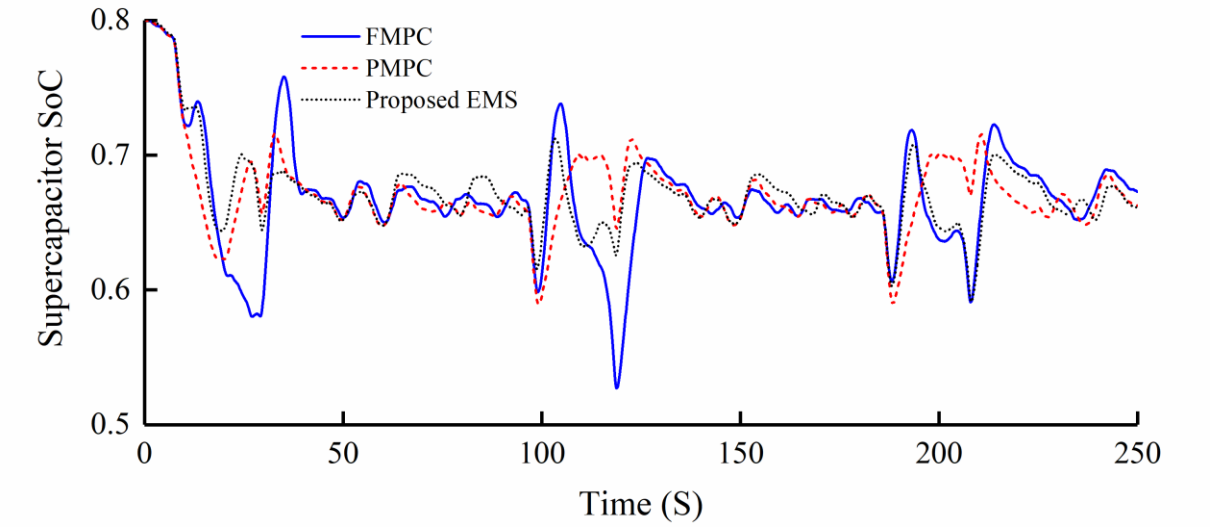

Figure 11. Supercapacitor SoC

Figure. 7 shows the FCS power. During the driving cycles, the FCS provided maximum power of 100 kW and minimum power of 10 kW. The FCS power is generally in the low power range. The peak power of FCS appears at heavy load conditions and lower battery/supercapacitor SoC conditions. The FCS power trajectories of FMPC and PMPC changes more frequently than that of proposed EMS. The FCS power of FMPC changes most frequently and fluctuates the most. This is because FMPC lacks prediction of working conditions, which leads to the difference between real demand power and predictive demand power (constant prediction). On contrast, PMPC exploits a priori knowledge of future conditions, which can fully deal with the change of operation conditions. Therefore, PMPC changes more than proposed EMS. It should be noted that the FCS power trajectory under the proposed EMS is less drastic, which means FCS durability can be effectively prolonged.

Figures. 8-9 show the battery power and battery SoC. The power spanned from -96.7 to 96.5 kW, and battery SoC correspondingly spanned from approximately 0.382 to 0.8. The trajectories of FMPC

have the minimum fluctuation range, which are -74.8 to 65 kW power range and 0.523 to 0.8 SoC range. The battery power and battery SoC trajectories of the proposed EMS are similar to that of the PMPC. Figures. 10-11 show the supercapacitor power and supercapacitor SoC, respectively. It is similar to that of battery performance that the trajectories of FMPC have the maximum fluctuation range and PMPC have the minimum fluctuation range. The range of FMPC are -146.1 to 98.9 kW power range and 0.527 to 0.8 SoC range, and the range of PMPC are -83.2 to 97.9 kW power range and 0.589 to 0.8 SoC range. Notably, the battery and supercapacitor trajectories are similar, with the proposed EMS between those of the others. In each cycle, the battery and supercapacitor SoC reach lower limits. The SoC of the power sources must be constrained especially during heavy load conditions for EMS development.

Simulation results show that the equivalent hydrogen consumption of the FMPC, PMPC, and proposed EMS are 242.94 g, 230.7 g, and 232.16 g, respectively. The equivalent hydrogen consumption has already included the changes in battery and supercapacitor relative to the initial state. Therefore, the proposed EMS can effectively save 4.43 % hydrogen consumption compared with FMPC, and is quite close to PMPC.

Seen as a whole, the proposed EMS excels FMPC and approximate to PMPC. Thus, the proposed EMS demonstrates good cost economy and SoC operating range, confirming its superiority. One of the advantages of the proposed EMS is the reduction in battery contribution and the increase of using supercapacitor. This advantage can be translated into an improvement in battery lifetime.

4. CONCLUSIONS

We developed an NSGA-II-optimised, multiobjective optimization predictive EMS for a fuel cell/battery/supercapacitor powered construction vehicle. Firstly, we described the FCHCV topology and modelled the power sources in detail. We then built an MOP model based on MPC theory. The predictive EMS sought to reduce costs and prolong fuel cell durability and battery lifetime. NSGA-II allows for trade-off between cost and performance. An NSGA-II-optimised multiobjective optimization system was used to generate a Pareto front and obtain optimal control solutions. The numerical results showed that NSGA-II yielded feasible solutions exhibiting a good spread that effectively converged to the non-dominated front. NSGA-II will aid the development of more complex MOPs. Finally, we employed a representative driving cycle to evaluate the effectiveness of our new EMS, using dynamic programming and weighted predictive EMSs as benchmarks. MATLAB simulations showed that our EMS reasonably distributed energy between different power sources, thus reducing costs and extending the power sources durability, and increasing system efficiency. Future research should focus on parameter optimisation and energy management of hybrid construction vehicles.

ACKNOWLEDGEMENT
This work was supported by the National Natural Science Foundation of China (Grant No. 51805200).

References

1. G. Wang, Y. Yu, H. Liu, C. Gong, S. Wen, X. Wang, Z. Tu, *Fuel Process. Technol.*, 179 (2018) 203–228.
2. T. Li, H. Liu, D. Ding, *Energy*, 149 (2018) 718–729.
3. Y. Ruf, Development of Business Cases for Fuel Cells and Hydrogen Applications for Regions and Cities, (2017) Brussels and Frankfurt.
4. A. Lajunen, *SAE Tech. Pap.* (2015) 2015-01–2829.
5. C. LEONIDA, *Intell. Min.* (2019) 1–3.
6. H. Jiang, L. Xu, J. Li, Z. Hu, M. Ouyang, *Energy*, 177 (2019) 386–396.
7. Q. Li, T. Wang, C. Dai, W. Chen, L. Ma, *IEEE Trans. Veh. Technol.*, 67 (2018) 5658–5670.
8. H. El Fadil, F. Giri, J.M. Guerrero, A. Tahri, *IEEE Trans. Veh. Technol.*, 63 (2014) 3011–3018.
9. V.K.R. Kasimalla, G. Naga Srinivasulu, V. Velisala, *Int. J. Energy Res.*, 42 (2018) 4263–4283.
10. Z. Fu, L. Zhu, F. Tao, P. Si, L. Sun, *Int. J. Hydrogen Energy*, 45 (2020) 8875–8886.
11. M. a. Hannan, F. a. Azidin, a. Mohamed, *Renew. Sustain. Energy Rev.*, 29 (2014) 135–150.
12. K. Gokce, A. Ozdemir, *Int. J. Electrochem. Sci.*, 11 (2016) 1228–1246.
13. Y. Wang, Z. Sun, Z. Chen, *Appl. Energy*, 254 (2019) 113707.
14. K. Song, F. Li, X. Hu, L. He, W. Niu, S. Lu, T. Zhang, *J. Power Sources*, 389 (2018) 230–239.
15. Q. Li, W. Yang, L. Yin, W. Chen, *IEEE Trans. Transp. Electrif.*, 6 (2020) 288–297.
16. Q. Li, H. Yang, Y. Han, M. Li, W. Chen, *Int. J. Hydrogen Energy*, 41 (2016) 16148–16159.
17. J. Chen, C. Xu, C. Wu, W. Xu, *IEEE Trans. Ind. Informatics*, 14 (2018) 292–300.
18. Q. Zhang, *Int. J. Electrochem. Sci.*, 15 (2020) 10866–10884.
19. Q. Li, W. Chen, Y. Li, S. Liu, J. Huang, *Int. J. Electr. Power Energy Syst.*, 43 (2012) 514–525.
20. S. Hou, J. Gao, Y. Zhang, M. Chen, J. Shi, H. Chen, *Int. J. Hydrogen Energy*, 45 (2020) 21858–21872.
21. M. Carignano, V. Roda, R. Costa-Castello, L. Valino, A. Lozano, F. Barreras, *IEEE Access*, 7 (2019) 16110–16122.
22. Y. Wu, A. Ravey, D. Chrenko, A. Miraoui, *Energy Convers. Manag.*, 196 (2019) 878–890.
23. X. Lü, Y. Wu, J. Lian, Y. Zhang, C. Chen, P. Wang, L. Meng, *Energy Convers. Manag.*, 205 (2020) 112474.
24. X. Li, Y. Wang, D. Yang, Z. Chen, *J. Power Sources*, 440 (2019) 227105.
25. H. Rezk, A.M. Nassef, M.A. Abdelkareem, A.H. Alami, A. Fathy, *Int. J. Hydrogen Energy*, 46 (2019) 6110–6126.
26. Q. Li, B. Su, Y. Pu, Y. Han, T. Wang, L. Yin, W. Chen, *IEEE Trans. Transp. Electrif.*, 5 (2019) 552–564.
27. D. Shen, C.C. Lim, P. Shi, *Control Eng. Pract.*, 98 (2020) 104364.
28. C. Bordons, F. Garcia-Torres, M.A. Ridao, Model Predictive Control of Microgrids, Springer, Cham, (2020).
29. Y. Huang, H. Wang, A. Khajepour, H. He, J. Ji, *J. Power Sources*, 341 (2017) 91–106.
30. J. Torreglosa, P. Garcia, L. Fernandez, F. Jurado, *IEEE Trans. Ind. Informatics*, 10 (2013) 1–1.
31. T. Li, L. Huang, H. Liu, *Energy*, 172 (2019) 840–851.
32. T. Li, H. Liu, H. Wang, Y. Yao, *IEEE Access*, 8 (2020) 25927–25937.
33. S. Ahmadi, S.M.T. Bathaee, A.H. Hosseinpour, *Energy Convers. Manag.*, 160 (2018) 74–84.
34. U. Sarma, S. Ganguly, *J. Energy Storage*, 19 (2018) 247–259.
35. Y. Collette, P. Siarry, Optimisation Multiobjectif: Algorithmes, Editions Eyrolles, (2011).
36. F. Ben Aicha, F. Bouani, M. Ksouri, *Int. J. Appl. Math. Comput. Sci.*, 23 (2013) 35–45.
37. H. Zhang, J. Yang, J. Zhang, P. Song, M. Li, *Proc. Inst. Mech. Eng. Part F J. Rail Rapid Transit*, 234 (2020) 511–523.
38. Y. Li, Y. Wu, Y. Zhang, S. Wang, *Int. J. Hydrogen Energy*, 44 (2019) 29658–29670.
39. K. Deb, A. Pratap, S. Agarwal, T. Meyarivan, *IEEE Trans. Evol. Comput.*, 6 (2002) 182–197.

40. M.H. Arshad, M.A. Abido, A. Salem, A.H. Elsayed, *IEEE Access*, 7 (2019) 177595–177606.
41. H. Sun, Z. Fu, F. Tao, L. Zhu, P. Si, *J. Power Sources*, 455 (2020) 227964.
42. A. Mahmoudzadeh Andwari, A. Pesiridis, S. Rajoo, R. Martinez-Botas, V. Esfahanian, *Renew. Sustain. Energy Rev.*, 78 (2017) 414–430.
43. T. Mesbahi, N. Rizoug, P. Bartholomëus, R. Sadoun, F. Khenfri, P. Le Moigne, *IEEE Trans. Ind. Electron.*, 65 (2018) 1298–1305.
44. M. Daowd, N. Omar, J. Van Mierlo, P. Van Den Bossche, *Int. Rev. Electr. Eng.*, 6 (2011) 1264–1278.
45. M. Daowd, N. Omar, J. Van Mierlo, P. Van Den Bossche, *Int. Rev. Electr. Eng.*, 6 (2011) 1692–1706.
46. T.C. Do, H.V.A. Truong, H.V. Dao, C.M. Ho, X.D. To, T.D. Dang, K.K. Ahn, *Energies*, 12 (2019) 4362.
47. H.V.A. Truong, H.V. Dao, T.C. Do, C.M. Ho, X.D. To, T.D. Dang, K.K. Ahn, *Energies*, 13 (2020) 3387.
48. Z. Bououchma, J. Sabor, H. Aitbouh, *Mater. Today Proc.*, 13 (2019) 688–697.
49. H. Fathabadi, *Energy*, 143 (2018) 467–477.
50. X. Wang, J. Chen, S. Quan, Y.X. Wang, H. He, *Appl. Energy*, 276 (2020) 115460.
51. C. Xiang, F. Ding, W. Wang, W. He, *Appl. Energy*, 189 (2017) 640–653.
52. Amin, R.T. Bambang, A.S. Rohman, C.J. Dronkers, R. Ortega, A. Sasongko, *IEEE Trans. Ind. Informatics*, 10 (2014) 1992–2002.
53. P.R.U. Guazzelli, W.C. De Andrade Pereira, C.M.R. De Oliveira, A.G. De Castro, M.L. De Aguiar, *IEEE Trans. Power Electron.*, 34 (2019) 6628–6638.
54. R. Tanabe, H. Ishibuchi, *Appl. Soft Comput. J.*, 89 (2020) 106078.
55. H. Wang, M. Olhofer, Y. Jin, *Complex Intell. Syst.*, 3 (2017) 233–245.
56. A. Kumar, R. Saxena, A. Kumar, *Proc. 2014 Int. Conf. Issues Challenges Intell. Comput. Tech. ICICT 2014* (2014) 109–112.
57. M. Elarbi, S. Bechikh, A. Gupta, L. Ben Said, Y.S. Ong, *IEEE Trans. Syst. Man, Cybern. Syst.*, 48 (2018) 1191–1210.
58. J.X. Wang, D.P. Gong, Y.S. Zhang, J.Y. Deng, Y. Shen, *Jilin Daxue Xuebao (Gongxueban)/Journal Jilin Univ. (Engineering Technol. Ed.*, 41 (2011) 27–33.
59. F. Odeim, J. Roes, A. Heinzel, *Energies*, 8 (2015) 6302–6327.